Inorganic Chemistry

Communication

Cite This: Inorg. Chem. 2017, 56, 13638-13641

pubs.acs.org/IC

Catalytic Water Oxidation by a Bio-inspired Nickel Complex with a Redox-Active Ligand

Dong Wang* and Charlie O. Bruner†

Department of Chemistry and Biochemistry and Center for Biomolecular Structure and Dynamics, University of Montana, Missoula, Montana 59812, United States

Supporting Information

ABSTRACT: The oxidation of water (H_2O) to dioxygen (O_2) is important in natural photosynthesis. One of nature's strategies for managing such multi-electron transfer reactions is to employ redox-active metal−organic cofactor arrays. One prototype example is the copper tyrosinate active site found in galactose oxidase. In this work, we have implemented such a strategy to develop a bio-inspired nickel phenolate complex capable of catalyzing the oxidation of H_2O to O_2 electrochemically at neutral pH with a modest overpotential. Employment of the redox-active ligand turned out to be a useful strategy to avoid the formation of high-valent nickel intermediates while a reasonable turnover rate (0.15 s^{-1}) is retained.

The oxidation of water (H_2O) to dioxygen (O_2) is an energetically uphill reaction (E° = +1.23 V vs NHE at pH 0) responsible for providing 99% of the driving force for natural photosynthesis.[1] This process occurs at the $CaMn_4O_4$ oxygen-evolving complex upon the accumulation of four oxidizing equivalents in a single turnover,[2] a strategy that minimizes extra energy input (overpotential)[3] and avoids the formation of partially oxidized product(s) [e.g., hydrogen peroxide (H_2O_2)]. One of the great challenges in the development of efficient artificial water oxidation electrocatalysts is to manipulate the driving force of the catalytic cycle close to the thermodynamic surface of water oxidation while retaining a reasonable turnover rate.

For single-site, homogeneous transition-metal-based electrocatalysts, most efforts have focused on systems where the metal is the only site for the storage of oxidizing equivalents,[4] while a few examples are available with both the metal and a redox-active ligand involved in the catalytic cycle.[5] To date, a system where the redox potentials of the metal and ligand could be modulated independently has yet to be reported.

We took inspiration from galactose oxidase (GAO), a mononuclear copper enzyme that catalyzes the two-electron oxidation of a range of primary alcohols to their corresponding aldehydes with the concomitant reduction of O_2 to H_2O_2.[6] The key redox-active component is a copper(I) tyrosinate, which is oxidized by two electrons to generate a copper(II) tyrosyl radical as the reactive oxidant (Scheme 1A). This example of synergy between a metal and an organic radical provides a useful strategy for mediating multi-electron transfer chemistry. In this work, we implemented this strategy to develop a bio-inspired nickel-phenolate complex capable of catalyzing water oxidation

Scheme 1. Key Redox-Active Species Involved in the Catalytic Cycle of (A) GAO and (B) the Nickel-Phenolate Complex 1 Studied in This Work

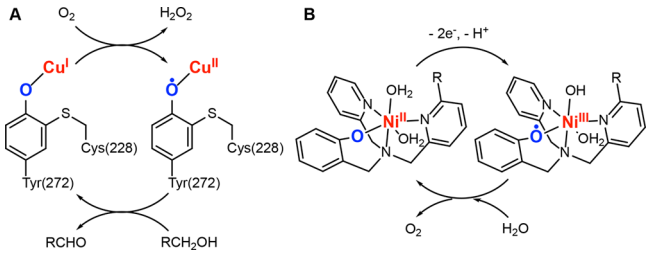

electrochemically at neutral pH and a moderate overpotential and demonstrated that both redox-active sites were utilized to store and transfer oxidizing equivalents in the catalytic cycle (Scheme 1B). Our findings have thus provided new insights into the rational design of molecular water oxidation electrocatalysts.

The complex Ni^{II}-L1 (**1**) can be synthesized by the reaction of 1:1 nickel(II) salt and ligand L1 (Scheme S1 and Figure S1) in wet tetrahydrofuran in the presence of 1 equiv of tetrabutylammonium hydroxide to deprotonate the phenol oxygen-donor. The crystal structure of **1** (Figure 1) shows that the tetradentate ligand L1 supports the formation of a mononuclear octahedral nickel(II) complex with two H_2O molecules bound in a cis configuration. The Ni−O bond distance of 2.061 Å for the phenolate oxygen-donor compares favorably with the ones reported for other phenolate ligands.[7] Notably, we found that a slight decrease of the steric hindrance from mesityl to 4-fluorophenyl (Figure S2) led to the formation of a dinuclear nickel complex $(Ni^{II}\text{-L2})_2$ (**2**), in which each phenolate acts as a bridging instead of a terminal ligand (Figure S3), even when the synthesis was carried out under identical conditions. Such a bis(phenolate)-bridged dinuclear structure has been widely observed in copper-phenolate complexes.[6c,8]

The optical spectrum of **1** in CH_3CN exhibited two primary absorptions at 309 nm (ε = 4200 M^{-1} cm^{-1}) and 385 nm (sh, ε = 650 M^{-1} cm^{-1}) and two weak peaks at 596 nm (ε = 14 M^{-1} cm^{-1}) and 950 nm (ε = 22 M^{-1} cm^{-1}) (Figure S4). These features resemble the ones reported for other nickel-phenolate complexes.[7,9] The absorption at 309 nm is assignable to the phenolate-to-nickel charge transfer transition.[9] When the spectrum was measured in buffered H_2O at pH ≥ 7, this band underwent a blue shift and became a shoulder at 296 nm (ε =

Received: August 30, 2017
Published: November 3, 2017

DOI: 10.1021/acs.inorgchem.7b02166
Inorg. Chem. 2017, 56, 13638−13641

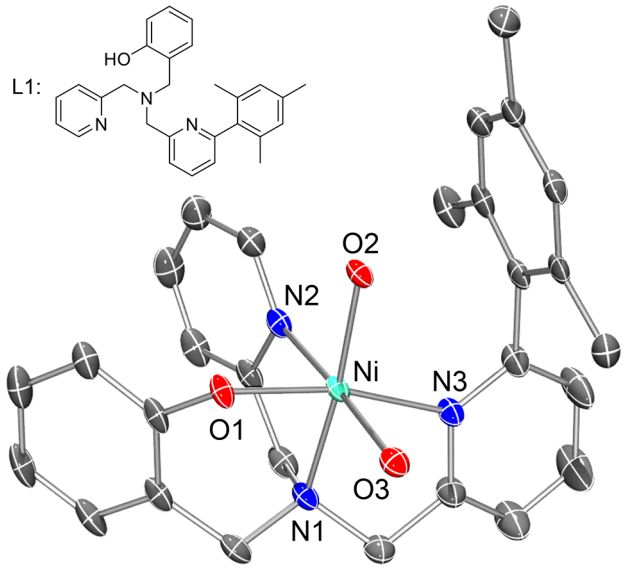

Figure 1. Crystal structure of **1** with thermal ellipsoids drawn at the 50% probability level. Hydrogen atoms are omitted for clarity. Selected bond distances (Å): Ni–O1, 2.061(1); Ni–O2, 2.048(1); Ni–O3, 2.125(2); Ni–N1, 2.086(2); Ni–N2, 2.066(2); Ni–N3, 2.156(2).

3200 M^{-1} cm^{-1}; Figure S5). This feature began to lose its intensity at pH < 7, suggesting that the phenolate was protonated at low pH. A pK_a of 6.2 was obtained for the phenolate oxygen-donor by a pH titration experiment (Figure S5).

The cyclic voltammogram (CV) of **1** in a sodium phosphate (Na-Pi) aqueous buffer at pH 7 using a glassy carbon working electrode (surface area ~0.07 cm^2) showed a strong, irreversible catalytic current with an onset potential of ~1200 mV vs Ag/AgCl reference (Figure 2, red). The catalytic current has a linear

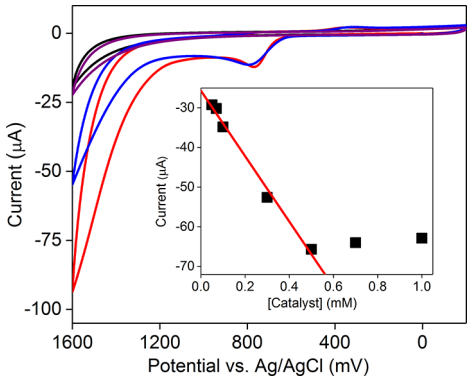

Figure 2. CVs of a 0.1 M Na-Pi buffer at pH 7 (black), 0.5 mM **1** in H_2O (red) and D_2O (blue), and a clean buffer using the working electrode removed from a 0.5 mM **1** containing solution (purple). Scan rate = 100 mV s^{-1}. Inset: Plot of the catalytic current at 1500 mV vs [**1**]. The red line represents the best linear fit up to [**1**] = 0.5 mM.

dependence on the concentration of **1** in the range of 0.05–0.5 mM (Figure 2, inset), suggesting that **1** is a single-site catalyst in an aqueous solution. The catalytic current became saturated at a catalyst loading higher than 0.5 mM. This observation is similar to that of a copper bipyridine water oxidation catalyst recently reported.[10] CV carried out in D_2O shows a much smaller catalytic current (Figure 2, blue), suggesting that the transfer of proton(s) from H_2O is a significant component of the rate-determining step. A solvent kinetic isotope effect (KIE) of 3.3 was determined according to eq 1.[5d,11] When CV of the clean buffer was performed using the working electrode removed from the catalyst-containing solution after gentle washing (see the Supporting Information for details),[12] no catalytic current was observed (Figure 2, purple), indicating that there is no deposit of a heterogeneous layer on the surface of the working electrode. On the other hand, complex **2** showed a lower catalytic activity than **1**.

$$\mathrm{KIE} = k_{\mathrm{cat,H_2O}}/k_{\mathrm{cat,D_2O}} = (i_{\mathrm{cat,H_2O}}/i_{\mathrm{cat,D_2O}})^2 \quad (1)$$

When normalized on the basis of the square root of the scan rate ($\nu^{-1/2}$), the catalytic current decreased upon an increase of the scan rate from 50 to 500 mV s^{-1} (Figure S6). Together with the notable KIE, these results suggested that the attack of H_2O to form an O–O bond by an active oxidant is the rate-determining step in the catalytic cycle. The turnover frequency (k_{obs}) was determined to be 0.15 s^{-1} by a widely used method described previously[5d] based on eq 2 (Figure S6, inset)

$$i_{cat}/i_{diff} = 2.24n(RTk_{obs}/F\nu)^{1/2} \quad (2)$$

where n = 4 and i_{cat} and i_{diff} represent the catalytic current of water oxidation and the diffusional current of the $PhO^{\bullet}/PhO^{-}$ couple (see below), respectively. This value compares favorably with those reported for other nickel-based water oxidation catalysts at neutral pH.[5b,13]

A solution containing 0.5 mM **1** in a Na-Pi buffer at pH 7 was then subjected to bulk electrolysis using an indium–tin oxide (ITO) working electrode (surface area ~7 cm^2). We applied a potential that is more positive than the onset potential to ensure fast production of O_2. As shown in Figure S7, the current obtained in the presence of **1** was much larger than that in the solution containing the buffer alone. No lag period was observed, indicating that the catalytic activity was not a result of the decomposed species of **1**. The Faradaic yield of O_2 formation was determined using a Clark electrode to be 80–90% (Figure S8). Importantly, we performed another electrolysis of the clean buffer solution using the working electrode (Figure S9) removed from the catalyst-containing solution after 30 min of electrolysis. No significant current was observed relative to a freshly prepared electrode (Figure S7, blue). These observations confirm that there is no formation of a heterogeneous nickel oxide layer at the surface of the ITO electrode.

We also studied the electrochemical properties of $Ni(NO_3)_2$, which is known to form heterogeneous nickel oxides active in catalyzing water oxidation at alkaline pHs.[14] As shown in Figure S10, CV of 0.5 mM $Ni(NO_3)_2$ in a Na-Pi buffer at pH 7 exhibited distinctly different behavior compared to that of **1**. In the forward scan, a catalytic current was not observed until the potential reached ~1500 mV, which is ~300 mV higher than the onset potential found for **1**. Moreover, a crossover catalytic wave and a broad cathodic feature at ~950 mV were observed on the reverse scan. In addition, we carried out bulk electrolysis of 0.5 mM $Ni(NO_3)_2$ at pH 7 using an ITO electrode. There is clear formation of a black nickel oxide layer on the electrode surface after electrolysis (Figure S9). Taken together, these results demonstrated that **1** is a homogeneous catalyst but not the precursor of a heterogeneous nickel oxide species.

At low potential, a non-catalytic anodic peak was observed at $E_{p,a}$ = 780 mV, which could be assigned to the oxidation of phenolate to the phenoxyl radical (Figure S11).[6c,7] This process is partially reversible, as revealed by the reverse scan even when the forward scan returned at 1000 mV, showing first a cathodic

DOI: 10.1021/acs.inorgchem.7b02166
Inorg. Chem. 2017, 56, 13638–13641

peak at $E_{p,c}(1)$ = 720 mV. The peak separation of 60 mV is indicative of a one-electron process; however, the reduced peak current compared to that of the anodic peak suggested that there is another process following the oxidation of phenolate. Additionally, there is a second cathodic peak at $E_{p,c}(2)$ = 350 mV. It is well-known that the phenoxyl radical could be stabilized through delocalization over the entire phenol ring.[6c] We thus attribute $E_{p,c}(2)$ to the one-electron reduction of the delocalized radical species.

In order to probe the mechanism of water oxidation catalysis, we carried out more CV studies in aqueous solutions buffered at a range of pHs from 7 to 11. As shown in Figures S12 and S13, the non-catalytic anodic peak is insensitive to the pH of the solution, consistent with our assignment of this feature to the $PhO^{\bullet}/PhO^{-}$ couple. In contrast, the onset potential for the catalytic process decreased with increasing pH. A plot of the potential measured at a constant current (e.g., −40 μA) as a function of the pH (Figure S12, inset) is linear with a slope of −60 mV/pH, indicating that generation of the reactive species for attacking H_2O is a metal-based one-electron process coupled with the transfer of one proton.

We thus propose a mechanism to summarize the key experimental findings (Scheme 2). Overall, the starting nickel-

Scheme 2. Proposed Water Oxidation Mechanism Catalyzed by 1

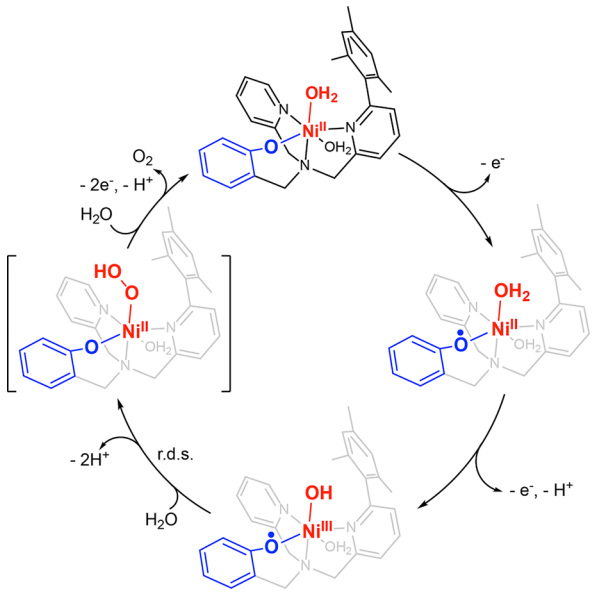

(II)-phenolate complex was oxidized by two one-electron steps to generate the reactive oxidant, a nickel(III) phenoxyl radical species. Both the solvent H/D KIE and the scan rate dependence studies demonstrated that the rate-determining step is the O−O bond formation. The resulting hydroperoxide intermediate likely continues to be oxidized on the electrode surface to produce O_2. Notably, **1** takes advantage of the phenolate ligand as the second redox-active site besides the metal center. Therefore, formation of a putative high-valent nickel−oxo species as the reactive intermediate[15] could be avoided, while a reasonable turnover rate is retained. On the other hand, **1** has limited stability under catalytic conditions, as revealed in Figure S7. This is likely due to the facts that (1) the phenolate moiety in ligand L1 has unsubstituted ortho and para positions susceptible to decomposition of the phenoxyl radical and (2) oxidation of the phenolate ligand occurs prior to that of the metal, which grants sufficient time for decomposition of the phenoxyl radical to take place. Further studies are aimed at exploring possible decomposition pathways of **1**[16] and enhancing its stability through modification of the ligand L1.

In conclusion, we have provided a proof-of-concept demonstration that a nickel-phenolate complex, **1**, could act as a single-site, molecular catalyst for the oxidation of H_2O to O_2 at neutral pH and a modest overpotential. Several lines of evidence have confirmed the homogeneous nature of **1** during catalysis. Both the metal and phenolate ligand were utilized to store and transfer oxidizing equivalents in the catalytic cycle, an advantageous strategy to avoid the formation of high-valent nickel intermediates. Furthermore, the flexibility of the ligand scaffold has provided unprecedented opportunities to modulate the redox properties of the metal and ligand individually to improve the catalytic activity, energy efficiency, and catalyst stability in future studies.

■ ASSOCIATED CONTENT

Supporting Information

The Supporting Information is available free of charge on the ACS Publications website at DOI: 10.1021/acs.inorgchem.7b02166.

Experimental methods, Scheme S1, and Figures S1−S13 (PDF)

Accession Codes

CCDC 1571238−1571239 contain the supplementary crystallographic data for this paper. These data can be obtained free of charge via www.ccdc.cam.ac.uk/data_request/cif, or by emailing data_request@ccdc.cam.ac.uk, or by contacting The Cambridge Crystallographic Data Centre, 12 Union Road, Cambridge CB2 1EZ, UK; fax: +44 1223 336033.

■ AUTHOR INFORMATION

Corresponding Author

*E-mail: dong1.wang@umontana.edu.

ORCID

Dong Wang: 0000-0002-6370-1942

Present Address

†Victor High School, Victor, MT 59812.

Notes

The authors declare no competing financial interest.

■ ACKNOWLEDGMENTS

Support of this work was provided by the Center for Biomolecular Structure and Dynamics CoBRE (Grant NIGMS P20GM103546) and the University of Montana. C.O.B. thanks the M. J. Murdock Charitable Trust for a Partnership in Science award (2015409: JAT: 2/25/2016). We thank Daniel A. Decato for his assistance in solving the crystal structures.

■ REFERENCES

(1) Barber, J. Photosynthetic Energy Conversion: Natural and Artificial. *Chem. Soc. Rev.* **2009**, *38*, 185−196.

(2) Najafpour, M. M.; Renger, G.; Hołyńska, M.; Moghaddam, A. N.; Aro, E.-M.; Carpentier, R.; Nishihara, H.; Eaton-Rye, J. J.; Shen, J.-R.; Allakhverdiev, S. I. Manganese Compounds as Water-Oxidizing Catalysts: From the Natural Water-Oxidizing Complex to Nanosized Manganese Oxide Structures. *Chem. Rev.* **2016**, *116*, 2886−2936.

DOI: 10.1021/acs.inorgchem.7b02166
Inorg. Chem. 2017, 56, 13638−13641

(3) Yamamoto, M.; Tanaka, K. Artificial Molecular Photosynthetic Systems: Towards Efficient Photoelectrochemical Water Oxidation. *ChemPlusChem* **2016**, *81*, 1028−1044.
(4) (a) Blakemore, J. D.; Crabtree, R. H.; Brudvig, G. W. Molecular Catalysts for Water Oxidation. *Chem. Rev.* **2015**, *115*, 12974−13005. (b) Wasylenko, D. J.; Palmer, R. D.; Berlinguette, C. P. Homogeneous Water Oxidation Catalysts Containing a Single Metal Site. *Chem. Commun.* **2013**, *49*, 218−227. (c) Kärkäs, M. D.; Åkermark, B. Water Oxidation Using Earth-abundant Transition Metal Catalysts: Opportunities and Challenges. *Dalton Trans.* **2016**, *45*, 14421−14461. (d) Kärkäs, M. D.; Verho, O.; Johnston, E. V.; Åkermark, B. Artificial Photosynthesis: Molecular Systems for Catalytic Water Oxidation. *Chem. Rev.* **2014**, *114*, 11863−12001. (e) Tong, L.; Thummel, R. P. Mononuclear Ruthenium Polypyridine Complexes that Catalyze Water Oxidation. *Chem. Sci.* **2016**, *7*, 6591−6603.
(5) (a) Garrido-Barros, P.; Funes-Ardoiz, I.; Drouet, S.; Benet-Buchholz, J.; Maseras, F.; Llobet, A. Redox Non-innocent Ligand Controls Water Oxidation Overpotential in a New Family of Mononuclear Cu-Based Efficient Catalysts. *J. Am. Chem. Soc.* **2015**, *137*, 6758−6761. (b) Han, Y.; Wu, Y.; Lai, W.; Cao, R. Electrocatalytic Water Oxidation by a Water-Soluble Nickel Porphyrin Complex at Neutral pH with Low Overpotential. *Inorg. Chem.* **2015**, *54*, 5604−5613. (c) Zhang, T.; Wang, C.; Liu, S.; Wang, J.-L.; Lin, W. A Biomimetic Copper Water Oxidation Catalyst with Low Overpotential. *J. Am. Chem. Soc.* **2014**, *136*, 273−281. (d) Wang, D.; Groves, J. T. Efficient Water Oxidation Catalyzed by Homogeneous Cationic Cobalt Porphyrins: Critical Roles for the Buffer Base. *Proc. Natl. Acad. Sci. U. S. A.* **2013**, *110*, 15579−15584. (e) Boyer, J. L.; Rochford, J.; Tsai, M.-K.; Muckerman, J. T.; Fujita, E. Ruthenium Complexes with Non-innocent Ligands: Electron Distribution and Implications for Catalysis. *Coord. Chem. Rev.* **2010**, *254*, 309−330. (f) Kärkäs, M. D.; Liao, R.-Z.; Laine, T. M.; Åkermark, T.; Ghanem, S.; Siegbahn, P. E. M.; Åkermark, B. Molecular Ruthenium Water Oxidation Catalysts Carrying Non-Innocent Ligands: Mechanistic Insight through Structure−Activity Relationships and Quantum Chemical Calculations. *Catal. Sci. Technol.* **2016**, *6*, 1306−1319.
(6) (a) Thomas, F. Ten Years of a Biomimetic Approach to the Copper(II) Radical Site of Galactose Oxidase. *Eur. J. Inorg. Chem.* **2007**, *2007*, 2379−2404. (b) Rogers, M. S.; Dooley, D. M. Copper-tyrosyl Radical Enzymes. *Curr. Opin. Chem. Biol.* **2003**, *7*, 189−196. (c) Jazdzewski, B. A.; Tolman, W. B. Understanding the Copper-phenoxyl Radical Array in Galactose Oxidase: Contributions from Synthetic Modeling Studies. *Coord. Chem. Rev.* **2000**, *200−202*, 633−685.
(7) Shimazaki, Y.; Huth, S.; Karasawa, S.; Hirota, S.; Naruta, Y.; Yamauchi, O. Nickel(II)-Phenoxyl Radical Complexes: Structure-Radical Stability Relationship. *Inorg. Chem.* **2004**, *43*, 7816−7822.
(8) Itoh, S.; Taki, M.; Fukuzumi, S. Active Site Models for Galactose Oxidase and Related Enzymes. *Coord. Chem. Rev.* **2000**, *198*, 3−20.
(9) Nagataki, T.; Ishii, K.; Tachi, Y.; Itoh, S. Ligand Effects on Ni^{II}-catalysed Alkane-hydroxylation with *m*-CPBA. *Dalton Trans.* **2007**, 1120−1128.
(10) Barnett, S. M.; Goldberg, K. I.; Mayer, J. M. A Soluble Copper-bipyridine Water-oxidation Electrocatalyst. *Nat. Chem.* **2012**, *4*, 498−502.
(11) Chen, Z.; Concepcion, J. J.; Hu, X.; Yang, W.; Hoertz, P. G.; Meyer, T. J. Concerted O Atom-proton Transfer in the O-O Bond Forming Step in Water Oxidation. *Proc. Natl. Acad. Sci. U. S. A.* **2010**, *107*, 7225−7229.
(12) Kaeffer, N.; Morozan, A.; Fize, J.; Martinez, E.; Guetaz, L.; Artero, V. The Dark Side of Molecular Catalysis: Diimine−Dioxime Cobalt Complexes Are Not the Actual Hydrogen Evolution Electrocatalyst in Acidic Aqueous Solutions. *ACS Catal.* **2016**, *6*, 3727−3737.
(13) Wang, J.-W.; Zhang, X.-Q.; Huang, H.-H.; Lu, T.-B. A Nickel(II) Complex as a Homogeneous Electrocatalyst for Water Oxidation at Neutral pH: Dual Role of HPO_4^{2-} in Catalysis. *ChemCatChem* **2016**, *8*, 3287−3293.
(14) Dincă, M.; Surendranath, Y.; Nocera, D. G. Nickel-borate Oxygen-evolving Catalyst that Functions under Benign Conditions. *Proc. Natl. Acad. Sci. U. S. A.* **2010**, *107*, 10337−10341.
(15) (a) Zhang, M.; Zhang, M.-T.; Hou, C.; Ke, Z.-F.; Lu, T.-B. Homogeneous Electrocatalytic Water Oxidation at Neutral pH by a Robust Macrocyclic Nickel(II) Complex. *Angew. Chem., Int. Ed.* **2014**, *53*, 13042−13048. (b) Luo, G.-Y.; Huang, H.-H.; Wang, J.-W.; Lu, T.-B. Further Investigation of a Nickel-Based Homogeneous Water Oxidation Catalyst with Two *cis*- Labile Sites. *ChemSusChem* **2016**, *9*, 485−491. (c) Wang, L.; Duan, L.; Ambre, R. B.; Daniel, Q.; Chen, H.; Sun, J.; Das, B.; Thapper, A.; Uhlig, J.; Dinér, P.; Sun, L. A Nickel (II) PY5 Complex as an Electrocatalyst for Water Oxidation. *J. Catal.* **2016**, *335*, 72−78.
(16) Kagalwala, H. N.; Tong, L.; Zong, R.; Kohler, L.; Ahlquist, M. S. G.; Fan, T.; Gagnon, K. J.; Thummel, R. P. Evidence for Oxidative Decay of a Ru-Bound Ligand during Catalyzed Water Oxidation. *ACS Catal.* **2017**, *7*, 2607−2615.

DOI: 10.1021/acs.inorgchem.7b02166
Inorg. Chem. 2017, 56, 13638−13641